# Design Optimization of a Semi-Active Haptic Feedback Device

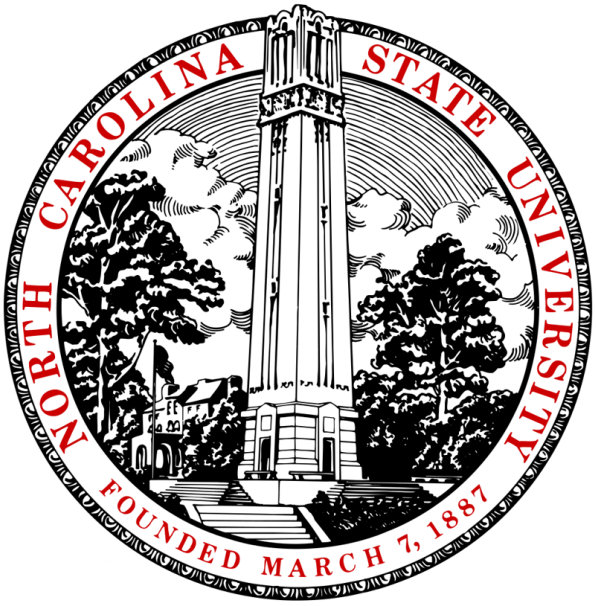


# Project Report

**Submitted by:**

**Vinod Kumar Singla (#200149761)**

**Bal Govind (#200161457)**

**Naveen Sankar (#200160717)**

# Contents

# List of Figures



# List of Tables

# 1. Problem Description and Magnetic Circuit Analysis

The design of the spool and cylinder is contingent on designer preferences and tradeoffs which are outlined below:

- The quantity of iron removed from the spool (to reduce weight) will affect the path of flux lines from the coil to the Magneto-Rheological Fluid (MRF) and baffle. As a later section on the Finite Element Analysis will show, if a relatively small quantity of iron is recovered to reduce the net weight of the device, the curvature of flux path-lines will be mostly unaffected. However, if a hole of relatively larger depth/ diameter is made in the spool, flux path length increases and may prove sub-optimal.

- As shown in Figure 1, the lengths of the spool and cylinder are decided based on the plausible travel of the lever in either direction. That is, for a lever of length, say, 12 inches with a travel of 4 inches in either direction and having a rod attached to the spool of 2 inches at the lever center, the cylinder length would be 6 inches. These values pose constraints which limit overall footprint of the device. Its dimensions were optimized to meet or exceed the performance specifications. Note, the inspiration behind 4-inch lever travel in either direction was taken from a typical mousepad which is about 8 inches in diameter.

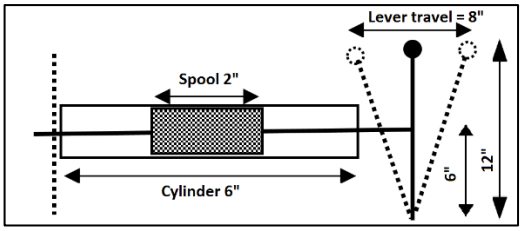


**Figure 1. Concept schematic illustrating degree of lever travel**

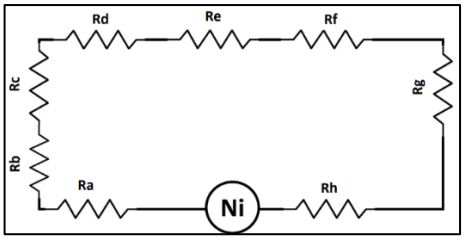


**Figure 2. Simplified circuit for MCA**

- To compute reluctance of the magnetic circuit for analysis, a simplified circuit (see Figure 2) consisting several individual reluctances in series was considered. In addition, to resolve the reluctance of individual elements, the total volume was segmented. This is shown in Figure 3. Sections for which areas vary or are complex to compute, an estimate was made by taking average of individual areas of respective starting and ending sections. The areas and mean path length thus computed for each segment are shown in Table 1.

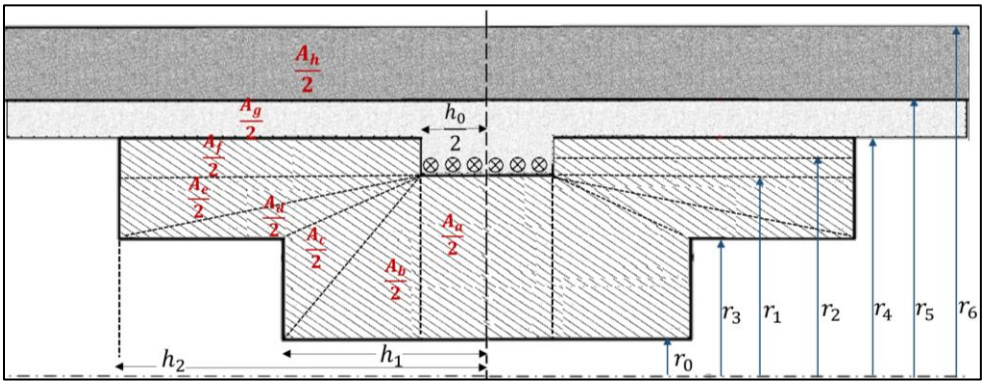


**Figure 3. Spool and cylinder half section**

**Table 1. Area & mean path length used to compute reluctance of segmented elements**

| Segment | Area of cross section ($A_x$) | Mean Path length ($L_x$) |
|---|---|---|
| **a** | $2\pi({r_1}^2 - {r_0}^2)$ | $h_0$ |
| **b** | $\pi({r_1}^2 - {r_0}^2 + (r_1 + r_0)\sqrt{(h_1)^2 + (r_1 - r_0)^2}\,)$ | $h_1$ |
| **c** | $\pi((r_1 + r_0)\sqrt{(h_1)^2 + (r_1 - r_0)^2} + (r_1 + r_3)\sqrt{(h_1)^2 + (r_1 - r_3)^2}\,)$ | $r_1 - r_3$ |
| **d** | $\pi(r_1 + r_3)(\sqrt{(h_1)^2 + (r_1 - r_3)^2}) + \sqrt{(h_2)^2 + (r_1 - r_3)^2}\,)$ | $h_2 - h_1$ |
| **e** | $\pi((r_1 + r_3)\sqrt{(h_2)^2 + (r_1 - r_3)^2} + 2r_1h_2)$ | $r_1 - r_3$ |
| **f** | $2\pi(r_4 + r_1)h_2$ | $2(r_4 - r_1)$ |
| **g** | $2\pi(r_4 + r_5)h_2$ | $2(r_5 - r_4)$ |
| **h** | $2\pi({r_6}^2 - {r_5}^2)$ | $h_0 + h_2$ |

In addition to no fringing & saturation assumptions, assuming fixed relative permeability of MRF ($\mu_{rm} = 4$) and iron ($\mu_{ri} = 5000$) for magnetic circuit analysis (MCA), an estimate of flux ($\Phi$) and consequently the flux density (B) in the MRF was made. The equations for the magnetic circuit can then be written as:

$$MMF = Ni = R\Phi \tag{1}$$

$$R = R_a + R_b + R_c + R_d + R_e + R_f + R_g + R_h \tag{2}$$

Substituting, we get,

$$Ni = \left[\frac{1}{\mu_0\mu_{rm}}\left(\frac{L_a}{A_a} + \frac{L_b}{A_b} + \frac{L_c}{A_c} + \frac{L_d}{A_d} + \frac{L_e}{A_e} + \frac{L_f}{A_f} + \frac{L_h}{A_h}\right) + \frac{1}{\mu_0\mu_{ri}}\left(\frac{L_g}{A_g}\right)\right]\Phi \tag{3}$$

The above equation was used to estimate flux density (B) for the optimized design illustrated in Table 4. This formulation was later validated using FEMM and Ansys Maxwell results. Here, the non-linear B-H curves (digitized from the project prompt's figures) and FEMM libraries were used for magnetostatic simulations.

# 2. Methodology

## 2.1 Design Optimization

There are several tradeoffs that exist between conflicting design requirements. Quantifying these tradeoffs is key to optimization problem setup. The objective function consists of damping force ($F_d$), total weight (M), input electrical energy ($W_s$), time constant ($\tau$), flux density (B) and penalty function (p). A high penalty (p = 1000) was added if the value of time constant exceeds 0.09 sec or if the on-state damping force exceeds 110N. The limits were intentionally set lower than the allowed max limits to account for modelling uncertainties. To prevent flux saturation, maximum magnetic field density was restricted to 1.5 Tesla. The input electrical energy & total weight terms were added to the objective function to penalize for increasing power utilization/weight. To ensure off state damping is less than 5 N, the gap was constrained to be

always greater than 1.5 mm. This ensures off-state damping force is almost zero. Different weighting factors were added to individual terms in the objective function to bring them around the same order of magnitude.

Since the objective function is highly non-linear, a robust heuristic search method – the genetic algorithm (GA), was used for optimization of design parameters. Based on an approximate overall cylinder width of 6 inches and spool width of 2 inches determined by the maximum lever travel, the upper and lower limits were imposed on the individual design parameters. It may be noted that the radii were constrained in a manner that always results in a feasible design. As explained in Section 1, we have chosen $r_3 \leq r_1$ and $h_1 \leq h_2$. This was done because removal of more material would contort flux path lines and considerably increase individual segments' reluctances. The optimization problem in standard form is given below:

$$Min.objF = p + 15M - F_d + W_s + 20 \times max.[B_{max} - 1.5, 0] \quad (4)$$

Subject to:

$g_1(x)$: $r_2 - r_1 \leq 3$ mm (5.a)

$g_2(x)$: $-r_2 + r_1 \leq -0.5$ mm (5.b)

$g_3(x)$: $r_3 - r_1 \leq 0$ (5.c)

$g_4(x)$: $-r_2 + r_4 \leq 2$ mm (5.d)

$g_5(x)$: $r_2 - r_4 \leq -1$ mm (5.e)

$g_6(x)$: $-r_4 + r_5 \leq 3$ mm (5.f)

$g_7(x)$: $r_4 - r_5 \leq -1.5$ mm (5.g)

$g_8(x)$: $-r_5 + r_6 \leq 10$ mm (5.h)

$g_9(x)$: $r_5 - r_6 \leq -2$ mm (5.i)

$g_{10}(x)$: $h_1 - h_2 \leq 0$ (5.j)

With upper and lower bounds on design variables:

$10 \text{ mm} < r_1 < 20 \text{ mm}$, $10.5 \text{ mm} < r_2 < 23 \text{ mm}$ , $0 \text{ mm} < r_3 < 20 \text{ mm}$,

$11 \text{ mm} < r_4 < 25 \text{ mm}$, $12 \text{ mm} < r_5 < 27 \text{ mm}$, $14 \text{ mm} < r_6 < 37 \text{ mm}$, (5.k)

$5 \text{ mm} < h_0 < 30 \text{ mm}$, $0 \text{ mm} < h_1 < 22.5 \text{ mm}$ and $5 \text{ mm} < h_2 < 22.5 \text{ mm}$

Material properties and supply voltage used for calculations are given in Table 2 and expressions for key design parameters are given in Table 3.

**Table 2. Material properties and supply voltage used for calculations**

| | |
|---|---|
| Electrical resistivity of copper | $\rho_e = 1.68 \times 10^{-8}\ \Omega.m$ |
| Density of iron | $\rho_i = 7.87 \times 10^3 kg/m^3$ |
| Density of copper | $\rho_c = 8.96 \times 10^3 kg/m^3$ |
| Permeability of free space | $\mu_0 = 1.25663706 \times 10^{-6}\ m.kg.s^{-2}A^{-2}$ |
| Supply Voltage | $V_s = 12\ V$ |

**Table 3. Expressions for key design parameters used for calculations**

| | |
|---|---|
| Damping force | $F_d(B,v) = \eta v \frac{A}{r_5 - r_4} + \tau_y(B)A$ |
| Area between lands of the piston | $A = 2\times\left(2\pi\frac{r_4 + r_5}{2}h_2\right)$ |
| Input electrical energy | $W_s = V_s I_s$ |
| Mass of the cylinder housing | $m_c = 3\pi(h_0 + 2h_2)({r_6}^2 - {r_5}^2)\rho_i$ |
| Mass of the spool | $m_s = \pi[(h_0 + 2h_2)({r_4}^2 - {r_0}^2) - 2h_1({r_3}^2 - {r_0}^2) - h_0({r_4}^2 - {r_1}^2)]\rho_i$ |
| Mass of the copper wire | $m_w = \frac{\pi}{4}{d_w}^2 l_w \rho_c$ |
| Number of turns of copper wire | $N_c = h_0\frac{(r_2 - r_1)}{{d_w}^2}$ |
| Length of copper wire | $l_w = 2\pi\frac{(r_1 + r_2)}{2}N_c$ |
| Total weight | $M = m_c + m_s + m_w$ |
| Time constant | $\tau = \frac{{N_c}^2}{RR_c}$ |
| Reluctance of the circuit | $R = \frac{1}{\mu_0\mu_{rm}}\left(\frac{L_a}{A_a} + \frac{L_b}{A_b} + \frac{L_c}{A_c} + \frac{L_d}{A_d} + \frac{L_e}{A_e} + \frac{L_f}{A_f} + \frac{L_h}{A_h}\right) + \frac{1}{\mu_0\mu_{ri}}\left(\frac{L_g}{A_g}\right)$ |
| Wire resistance | $R_c = \frac{4\rho_e l_w}{\pi {d_w}^2}$ |

The optimization algorithm was run several times and results were tabulated for each run (see **Appendix**). Since optimized design candidates meet or exceed stated specifications, the design with lowest size, mass and objective function value was selected as the final design. The final design dimensions were further rounded off to decrease the tolerance needed for machining and a non-significant variation in performance was observed. Table 4 shows the dimensions of the spool & cylinder for our optimized design and its specifications.

Another design optimization, wherein the on-state damping force was limited to 80 N instead of 110 N was considered to investigate the possibility of further reduction in mass of the device. It was observed that mass reduced 35.4% from 0.79Kg to 0.51Kg (see **Appendix**) while still meeting all other performance specifications. This demonstrates the tradeoff between on-state damping force and mass of the device and based on relative importance of these parameters for an application, specific design decisions can be made.

**Table 4. Optimized design dimensions and specifications**

| **Dimension (mm)** | **$r_1$** | **$r_2$** | **$r_3$** | **$r_4$** | **$r_5$** | **$r_6$** | **$h_0$** | **$h_1$** | **$h_2$** |
|---|---|---|---|---|---|---|---|---|---|
| **Value** | 13.6 | 16.4 | 7.4 | 17.4 | 18.9 | 23.3 | 13.8 | 9.5 | 12.7 |
| | | | | | | | | | |
| **Specification** | **τ (s)** | **Fd (N)** | **M (kg)** | **lw (m)** | **Vs (V)** | **Is (A)** | **Ws(W)** | **Nc** | **Rc (Ω)** |
| **Value** | 0.089 | 108.15 | 0.79 | 58.26 | 12 | 0.60 | 7.22 | 618 | 19.94 |
| | | | | | | | | | |
| **Specification** | **Ba (T)** | **Bb (T)** | **Bc (T)** | **Bd (T)** | **Be (T)** | **Bf (T)** | **Bg (T)** | **Bh (T)** | **objF** |
| **Value** | 1.49 | 1.33 | 1.17 | 1.03 | 0.858 | 0.70 | 0.598 | 1.49 | -89.04 |

## 2.2 Validation by Finite Element Analysis

To ensure accuracy of predicted magnetic field intensity (B) in the magnetorheological fluid (MRF) and performance specifications, both 2D and 3D finite element analysis (FEA) was done. Although a 2D FEA seems redundant, its predictions are essential to establish confidence in the design before a 3D FEA is attempted which is computationally expensive. The relative permeability of MRF ($\mu_{rm}$) was set to 5 for the simulation as per the predicted magnetic field from MCA. The results from 2D simulation performed in FEMM are shown in Figure 4(a) for a maximum damping force of 110N. This design had a calculated mass of 0.79 kg. Observably, the magnetic field in the MRF (0.6023 T) is within 3% of that predicted by MCA (0.598 T). Figure 4(b) shows another permutation in design wherein the maximum damping force was limited to 80N. For this design, calculated mass is 0.51 kg and the magnetic field in the MRF (0.6339 T) is again within 3% of that predicted by MCA (0.6453 T).

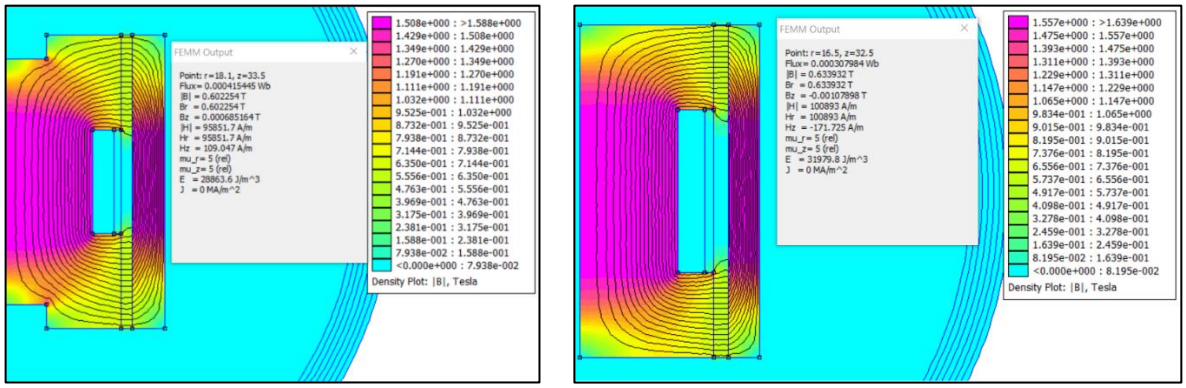


$F_{dmax}$ = 110 N, Mass = 0.79 Kg, B = 0.6023 T  $F_{dmax}$ = 80 N, Mass = 0.51 Kg, B = 0.6339 T

**Figure 4. FEMM analysis validates field intensity, B estimates by MCA**

The 3-D magneto-static analysis, using Ansys Maxwell, was then performed with an objective of finding the effective magnetic flux density in the region encompassed by the magnetorheological fluid. The geometry modelled in Maxwell 3-D modeler is shown in Figure 5. It was formed by the revolution of the individual components' cross-sections, which were parameterized. The excitation was defined at the cross-section of the coil in a circumferential direction. The dimensions of the computational domain ('Region') exceeded that of the device by 250 per cent in all axes to account for effects of fringing. Properties of the non-linear behavior of the MRF and pure iron were tabulated and incorporated into the B-H curves in the materials' database. The convergence criteria was uniform 0.5 percent of energy residuals for the cases considered. Convergence was achieved in about 15 iterative passes by progressively increasing tetrahedral grid size (364,000 cells).

The magnetic flux shows an abrupt rise in magnitude at the interface (i.e. at a radial distance of $r_5$). To account for this, we investigated the variance of flux through the radial gap filled by MRF between spool and the cylinder. As shown in Figure 6, the flux density shows small variation along the radial distance in the MRF between the $r_4$ and $r_5$. The non-linear relationship of the B-H curve bears this effect. The mean however, is 0.64 T which reasonably validates the predictions of the magnetic circuit analysis.

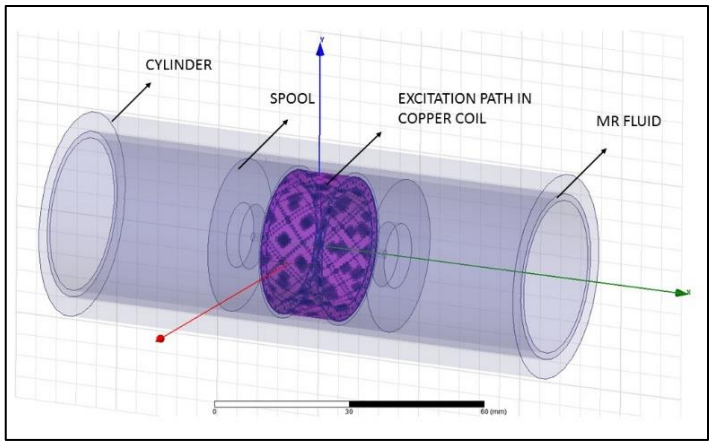


**Figure 5. Solid model of spool, cylinder housing and excitation path in coil**

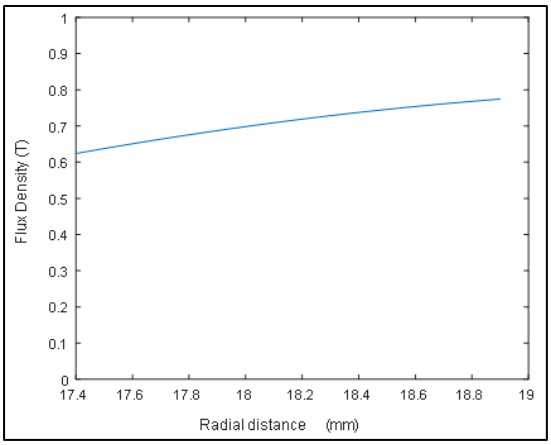


**Figure 6. Flux density variation in the MRF gap**

Contour plots (see Figures 7 (a) and (b)) reveal that fringing occurs along the edges of the radial conduction paths. Again, there is sharp rise in flux density at the interface of the MRF and the ferromagnetic cylinder.

Objectively, the non-linear B-H relationship causes the gradient in magnetic field, the mean of which corroborates the results of magnetic circuit analysis and 2-D FEMM analysis.

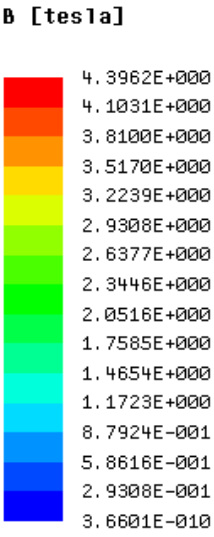


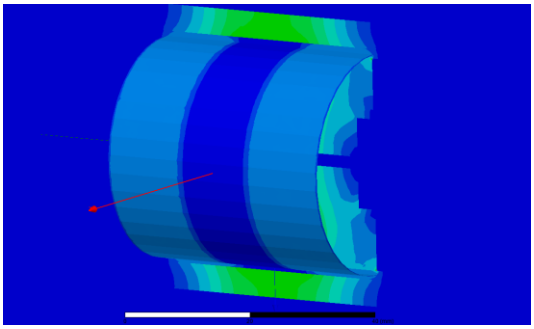

**Fig. 7 (a)**

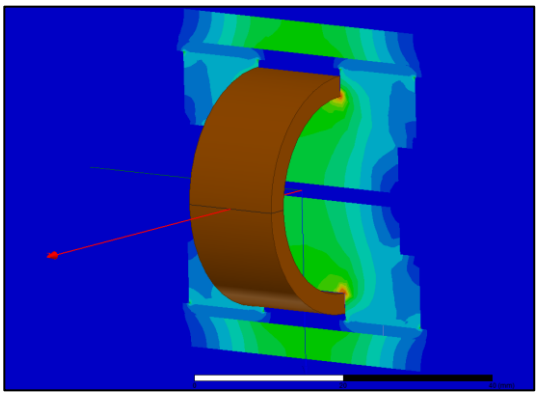

**Fig. 7 (b)**

**Figure 7 (a) Flux density through mid-surface of cylindrical MRF fluid volume, (b) Flux density through X-Y plane shows greater saturation near coil**

## 3. Performance characteristics due to variation in operating conditions and design parameters

The flexible design criteria give cause to further investigate the variation of damping force as a function of supply voltage. By supplying a transient sinusoidal voltage (Figure 8(b)) of $V_s = 6\,(1 + \sin(t))$, i.e. a variation from 0 V to 12 V in supply voltage amplitude, the effect of MRF's non-linear region of the B-H curve can be gleaned during the negative going portion of the cycle. A Simulink model (Figure 8 (a)) simplifies the task. As shown in Figure 8 (d), there is a deviation from one to one correlation between supply voltage and the associated damping force due to substantially reduced flux density in MRF (Figure 8 (c)) at lower supply voltage.

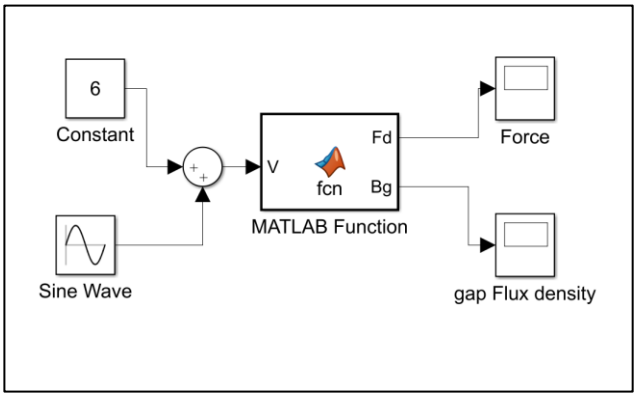


**Figure 8 (a). Simulink model for transient response of damping force**

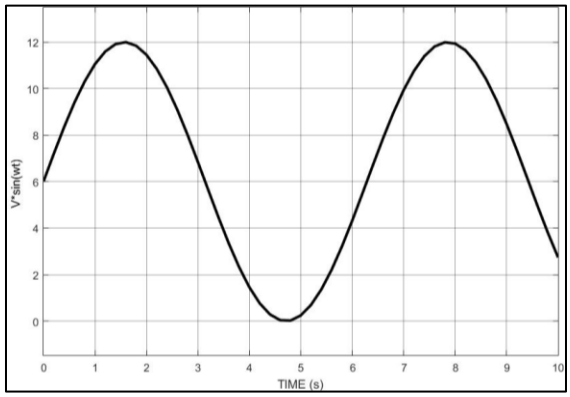


**Fig. 8 (b). Sinusoidal input voltage**

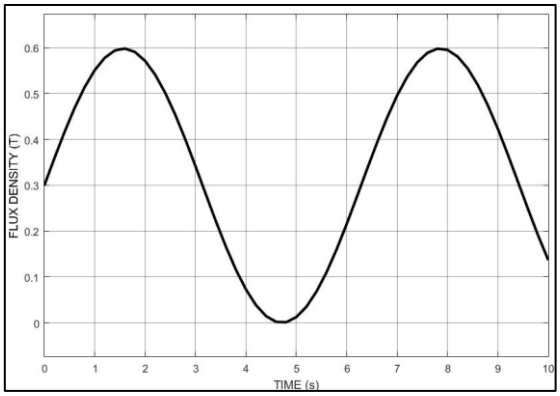


**Fig 8 (c). Time-transient response of flux density in MRF**

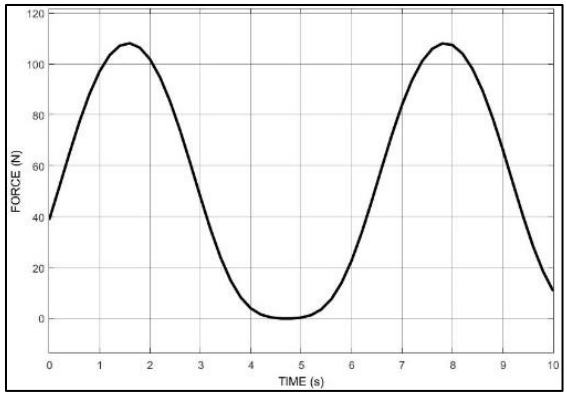


**Fig 8 (d). Time-transient response of damping force**

**Figure 8. Transient response of system characteristics**

The variation of damping force with respect to cylinder housing thickness is instructive. As Figure 9 shows, by increasing material in the cylinder housing manifested by increased radial thickness ($r_6$), flux density in the MRF and damping force are increased, albeit non-linearly. This gain is, however, at the expense of added weight to the device and increased time constant of resultant magnetic circuit.

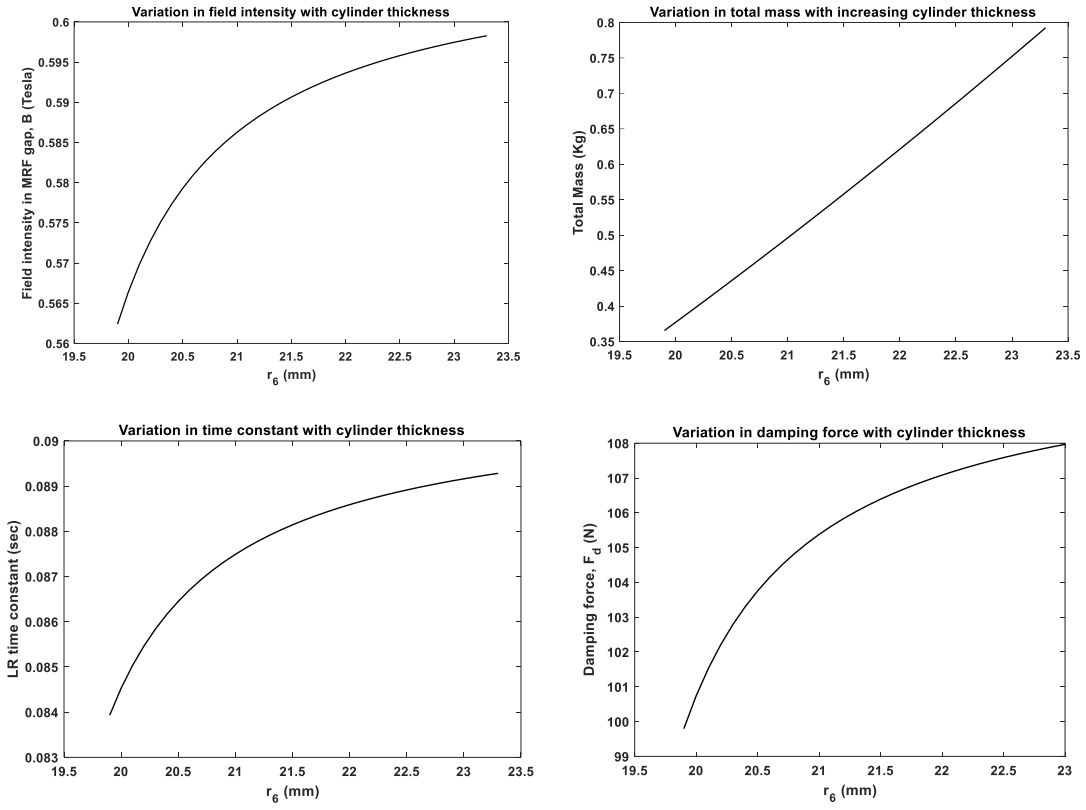


**Figure 9. Effect of cylinder thickness on damping force in the MRF and other key parameters**

# 4. Conclusion

The analysis techniques (MCA) and tools (FEMM, Maxwell) learned throughout the course were effectively utilized during this project. The tradeoff between damping force and mass of the device was illustrated by 1) considering different upper limits for damping force, 2) varying the cylinder thickness; and documenting resulting mass of the device for optimized design.

The non-linear behavior of the MRFs' B-H curve was demonstrated by considering the time transient response of flux density in the MRF with respect to a sinusoidal supply voltage.

All in all, the project was a resounding success since we could produce not one, but several design candidates with reasonable footprints that met or exceeded prescribed performance specifications.

***

## REFERENCES


[1] Hayt, William H., Jack E. Kemmerly, and Steven M. Durbin. *Engineering Circuit Analysis*. New York: McGraw-Hill, 2012.

[2] Fitzgerald, Arthur Eugene, Charles Kingsley, and Stephen D. Umans. *Fitzgerald & Kingsley's Electric Machinery*. New York: McGraw-Hill, 2014.

[3] User's guide – Maxwell 3D. Ansys (2010).

[4] Lord Corporation website: http://www.lord.com/products-and-solutions/steering-units (March 2015)

[5] Lord Corporation website: http://www.lord.com/products-and-solutions/active-vibrationcontrol/aerospace-and-defense/suspension-systems (March 2015).

[6] Mathworks website: https://www.mathworks.com/help/curvefit/index.html (April 2017)

[7] Elliot, Christopher Mark. PhD Thesis: Methods for Streamlined Firefly Optimization and Interpretation: Applications to Electromechanical Systems Design (Under the Direction of Gregory D. Buckner).

[8] Rohatgi, Ankit. "WebPlotDigitizer." *WebPlotDigitizer - Extract Data from Plots, Images, and Maps*.Jan. 2017. Web. 26 Apr. 2017. <http://arohatgi.info/WebPlotDigitizer/>.

[9] Jolly MR, Bender JW, Carlson JD, Properties and Applications of Commercial Magnetorheological Fluids, Lord Corporation.

# Appendix

## 1. Matlab Code for design optimization and curve fits:

```
% MAE 535 Design of Electromechanical Systems - Course Project
% Optimization for semi-haptic feedback device design
% Optimization_master.m    Vinod Kumar Singla 4/20/2017

clear all;clc;close all;
lb = [10;10.5;0;11;12;14;5;0;5]; % lower bounds on individual design variables
ub = [20;23;20;25;27;37;30;22.5;22.5]; % upper bounds on individual design variables
opts =
gaoptimset('PlotFcn',{@gaplotbestf,@gaplotstopping},'Generations',2000,'TolFun',1e-8);
fitnessfcn = @objF;
nvars = 9;
nonlcon = [];
Aeq = [];
beq = [];
A = [-1 1 0 0 0 0 0 0 0;1 -1 0 0 0 0 0 0 0;-1 0 1 0 0 0 0 0 0;...
    0 -1 0 1 0 0 0 0 0;0 1 0 -1 0 0 0 0 0;0 0 0 -1 1 0 0 0 0;...
    0 0 0 1 -1 0 0 0 0;0 0 0 0 -1 1 0 0 0;0 0 0 0 1 -1 0 0 0;...
    0 0 0 0 0 0 0 1 -1];
b = [3;-0.5;0;2;-1;3;-1.5;10;-2;0];
[x,fval,exitflag,output] = ga(fitnessfcn,nvars,A,b,Aeq,beq,lb,ub,nonlcon,opts)


% MAE 535 Design of Electromechanical Systems - Course Project
% Optimization for semi-haptic feedback device design
% objF.m Vinod Kumar Singla 4/20/2017

function f = objF(x)
%Note: x = [r1, r2, r3, r4, r5, r6, h0, h1, h2]
r1 = 1e-3*x(1);  r2 = 1e-3*x(2);  r3 = 1e-3*x(3);
r4 = 1e-3*x(4);  r5 = 1e-3*x(5);  r6 = 1e-3*x(6);
h0 = 1e-3*x(7);  h1 = 1e-3*x(8);  h2 = 1e-3*x(9);

% Data needed
r0 = 1e-3; % inner bore dia, m
rho_i = 7.87*10^3; % iron density, Kg/m^3
rho_c = 8.96*10^3; % copper density, Kg/m^3
dw = 25*1e-5; % copper wire dia, m
mu_0 = 1.25663706*1e-6; % Permeability of free space , m*kg*s^-2*A^-2
mu_ri = 5000; % Relative Permeability of iron, dimensionless
mu_rf = 4; % Relative Permeability of mrf, dimensionless
Nc = h0*(r2-r1)/dw^2; % Number of wire turns, dimensionless
Lw = 2*pi*Nc*(r1+r2)/2; % Wire length, m
Aw = pi*dw^2/4; % cross sectional area of wire, m^2
rhoe = 1.68*10^-8; % electrical resistivity of copper (ohm-m)
%yeta = 250; % dynamic viscosity of mrf, Pa-s, for v = 1 m/s
Rw = rhoe*Lw/Aw; % total wire resistance, ohms
Vs = 12; % Supply voltage, volts
Is = Vs/Rw; % current in the coil, amps
As = pi*(r4+r5)*h2*2; % area b/w lands of piston & cylinder wall, m^2
penalty = 0; % Will be increased for exceeding a certain preset # of turns
% mass calculation
mc = 3*pi*(r6^2-r5^2)*(h0+2*h2)*rho_i; % Cylinder mass, Kg, assuming cylinder length
to be 3 times to that of spool
ms = pi*((2*h2+h0)*(r4^2- r0^2)-2*h1*(r3^2-r0^2)-h0*(r4^2-r1^2))*rho_i;%Spool mass, Kg
mw = (pi/4)*dw^2*Lw*rho_c; % coil mass, Kg
M = mc+ms+mw; % Total mass of spool, cylinder and coil, Kg

% Magnetic circuit analysis (MCA) for calculating B in mrf
```

```
Aa = 2*pi*(r1^2-r0^2); La = h0;
Ab = pi*(r1^2-r0^2+(r1+r0)*sqrt(h1^2+(r1-r0)^2)); Lb = h1;
Ac = pi*((r1+r0)*sqrt(h1^2+(r1-r0)^2)+(r1+r3)*sqrt(h1^2+(r1-r3)^2)); Lc = r1-r3;
Ad = pi*(r1+r3)*(sqrt(h1^2+(r1-r3)^2)+sqrt(h2^2+(r1-r3)^2)); Ld = h2-h1;
Ae = pi*((r1+r3)*sqrt(h2^2+(r1-r3)^2)+2*r1*h2); Le = r1-r3;
Af = 2*pi*(r4+r1)*h2; Lf = 2*(r4-r1);
Ag = 2*pi*(r4+r5)*h2; Lg = 2*(r5-r4);
Ah = 2*pi*(r6^2-r5^2); Lh = h0+h2;
R = (La/Aa+Lb/Ab+Lc/Ac+Ld/Ad+Le/Ae+Lf/Af+Lh/Ah)/(mu_0*mu_ri)+(Lg/Ag)/(mu_0*mu_rf);
phi = Nc*Is/R; % flux in magnetic circuit, weber
Ba = phi/Aa; % flux density in mrf, Tesla
Bb = phi/Ab; % flux density in segment a, Tesla
Bc = phi/Ac; % flux density in segment a, Tesla
Bd = phi/Ad; % flux density in segment a, Tesla
Be = phi/Ae; % flux density in segment a, Tesla
Bf = phi/Af; % flux density in segment a, Tesla
Bg = phi/Ag; % flux density in segment a, Tesla
Bh = phi/Ah; % flux density in segment a, Tesla
B = [Ba,Bb,Bc,Bd,Be,Bf,Bg,Bh];
% damping force calculation
tauy_mrf = 1e3*(-103.4*Bg^3 + 152*Bg^2 + 8.548*Bg -0.04002); % shear yield of mrf, Pa
Fd = As*(tauy_mrf); % damping force, N, assuming a gap of >= 1.5 mm

% (LR) time constant
tau = Nc^2/(R*Rw);
% Objective function
if Fd>110
    Fd=-1000;
end

% Penalty for exceeding time constant
if tau>0.09
   penalty = 1000;
end

f = penalty + 15*M - Fd + Vs*Is + 20*max(max(B)-1.5,0); % note mass is multiplied with
a weighting factor to bring it closer to the same order of magnitude as damping force
end

% MAE 535 Design of Electromechanical Systems - Course Project
% Optimization for semi-haptic feedback device design
% Bvsmur_mrf_curvefit.m Vinod Kumar Singla 4/20/2017
function mu_r_mrf = Bvsmur_mrf_curvefit(B)
x = B;
p1  =     -4.968; p2  =     22.61;
p3  =     -36.64;p4  =      25.77;
p5  =     -11.1; p6  =     7.786;
mu_r_mrf = p1*x^5 + p2*x^4 + p3*x^3 + p4*x^2 + p5*x + p6;
end

% MAE 535 Design of Electromechanical Systems - Course Project
% Optimization for semi-haptic feedback device design
% Bvsshearyield_mrf_curvefit.m Vinod Kumar Singla 4/20/2017
function tauy_mrf = Bvsshearyield_mrf_curvefit(B)
x = B;
p1  =     -103.4;p2  =      152;
p3  =     8.548;p4  =    -0.04002;
tauy_mrf = p1.*x.^3 + p2.*x.^2 + p3.*x + p4;
end
```

## 2. Optimized designs for individual runs of genetic algorithm

Table 5. Optimized designs when upper limit for on-state damping is $F_{dmax} = 110\ N$

| DV | x1 | x2 | x3 | x4 | x5 | x6 | x7 | x8 | x9 | x10 |
|---|---|---|---|---|---|---|---|---|---|---|
| r1 | 13.41 | 13.27 | 15.47 | **13.59** | 13.59 | 13.48 | 13.55 | 13.59 | 13.59 | 13.44 |
| r2 | 15.32 | 15.21 | 17.96 | **16.42** | 16.34 | 15.63 | 15.83 | 16.27 | 16.30 | 15.81 |
| r3 | 13.36 | 4.32 | 9.78 | **7.40** | 6.16 | 13.48 | 13.55 | 3.57 | 11.04 | 3.90 |
| r4 | 16.50 | 16.21 | 19.12 | **17.43** | 17.42 | 16.63 | 16.95 | 17.27 | 17.34 | 16.81 |
| r5 | 18.01 | 17.71 | 20.69 | **18.93** | 18.92 | 18.13 | 18.46 | 18.77 | 18.84 | 18.31 |
| r6 | 22.43 | 22.11 | 24.94 | **23.28** | 23.27 | 22.57 | 22.87 | 23.15 | 23.20 | 22.69 |
| h0 | 20.57 | 20.31 | 14.89 | **13.79** | 14.15 | 18.23 | 17.24 | 14.55 | 14.40 | 16.57 |
| h1 | 12.72 | 4.71 | 4.43 | **9.47** | 5.37 | 12.79 | 12.67 | 5.71 | 12.25 | 5.65 |
| h2 | 12.74 | 12.91 | 14.30 | **12.68** | 12.67 | 12.79 | 12.67 | 12.78 | 12.64 | 12.81 |
| objF | -88.30 | -86.26 | -86.56 | **-89.05** | -88.72 | -89.09 | -89.56 | -88.47 | -89.65 | -87.66 |
| | | | | | | | | | | |
| Results | x1 | x2 | x3 | x4 | x5 | x6 | x7 | x8 | x9 | x10 |
| tau | 0.09 | 0.09 | 0.09 | **0.09** | 0.09 | 0.09 | 0.09 | 0.09 | 0.09 | 0.09 |
| mc | 0.61 | 0.60 | 0.63 | **0.53** | 0.54 | 0.59 | 0.58 | 0.55 | 0.54 | 0.56 |
| ms | 0.15 | 0.25 | 0.32 | **0.23** | 0.24 | 0.14 | 0.14 | 0.25 | 0.18 | 0.25 |
| mw | 0.03 | 0.02 | 0.03 | **0.03** | 0.03 | 0.03 | 0.03 | 0.03 | 0.03 | 0.03 |
| Lw | 56.86 | 56.28 | 62.09 | **58.83** | 58.69 | 57.48 | 57.92 | 58.53 | 58.68 | 57.63 |
| ls | 0.62 | 0.62 | 0.56 | **0.60** | 0.60 | 0.61 | 0.61 | 0.60 | 0.60 | 0.61 |
| Ba | 1.53 | 1.56 | 1.22 | **1.50** | 1.50 | 1.51 | 1.50 | 1.50 | 1.50 | 1.53 |
| Bb | 1.25 | 1.50 | 1.19 | **1.33** | 1.44 | 1.25 | 1.24 | 1.43 | 1.25 | 1.45 |
| Bc | 0.91 | 1.49 | 1.35 | **1.18** | 1.45 | 0.91 | 0.91 | 1.38 | 0.97 | 1.41 |
| Bd | 0.80 | 1.20 | 1.02 | **1.03** | 1.17 | 0.79 | 0.80 | 1.16 | 0.88 | 1.17 |
| Be | 0.80 | 0.88 | 0.70 | **0.86** | 0.87 | 0.79 | 0.80 | 0.88 | 0.83 | 0.88 |
| Bf | 0.72 | 0.72 | 0.59 | **0.70** | 0.70 | 0.71 | 0.71 | 0.70 | 0.70 | 0.71 |
| Bg | 0.62 | 0.62 | 0.51 | **0.60** | 0.60 | 0.62 | 0.61 | 0.60 | 0.60 | 0.61 |
| Bh | 1.53 | 1.56 | 1.50 | **1.50** | 1.50 | 1.51 | 1.50 | 1.50 | 1.50 | 1.53 |
| Fd | 108.00 | 108.01 | 108.00 | **107.99** | 107.99 | 108.01 | 108.00 | 108.00 | 108.00 | 108.00 |
| Nc | 629.85 | 629.00 | 591.25 | **623.98** | 624.12 | 628.56 | 627.47 | 623.98 | 624.93 | 627.13 |
| objF | -88.30 | -86.26 | -86.56 | **-89.05** | -88.72 | -89.10 | -89.56 | -88.47 | -89.65 | -87.66 |
| Rc | 19.46 | 19.26 | 21.25 | **20.14** | 20.09 | 19.67 | 19.82 | 20.03 | 20.08 | 19.72 |
| Ws | 7.40 | 7.48 | 6.78 | **7.15** | 7.17 | 7.32 | 7.26 | 7.19 | 7.17 | 7.30 |
| M | 0.79 | 0.88 | 0.98 | **0.79** | 0.81 | 0.75 | 0.75 | 0.82 | 0.75 | 0.84 |
| Ls | 46.05 | 46.14 | 43.49 | **39.15** | 39.48 | 43.81 | 42.57 | 40.11 | 39.69 | 42.18 |
| Lc | 138.14 | 138.42 | 130.48 | **117.44** | 118.44 | 131.42 | 127.72 | 120.33 | 119.07 | 126.55 |

Table 6. Optimized designs when upper limit for on-state damping is $F_{dmax} = 80\ N$

| DV | x1 | x2 | x3 | x4 | x5 | x6 | x7 | x8 | x9 | x10 |
|---|---|---|---|---|---|---|---|---|---|---|
| r1 | 12.00 | 11.63 | 12.86 | 11.74 | **11.82** | 11.58 | 11.68 | 11.65 | 11.65 | 12.88 |
| r2 | 14.22 | 14.27 | 15.40 | 14.00 | **14.79** | 13.83 | 14.27 | 13.55 | 14.35 | 15.49 |
| r3 | 11.97 | 11.63 | 4.08 | 9.36 | **11.82** | 11.58 | 10.40 | 11.42 | 11.60 | 3.15 |
| r4 | 15.22 | 15.27 | 16.50 | 15.02 | **15.80** | 14.83 | 15.27 | 14.55 | 15.36 | 16.51 |
| r5 | 17.19 | 16.93 | 18.96 | 16.80 | **17.38** | 16.44 | 16.98 | 16.26 | 17.04 | 18.31 |
| r6 | 20.92 | 20.51 | 22.88 | 20.47 | **20.88** | 20.08 | 20.58 | 19.97 | 20.61 | 21.85 |
| h0 | 22.72 | 20.18 | 17.14 | 23.12 | **18.06** | 23.77 | 20.49 | 27.99 | 19.69 | 19.33 |
| h1 | 12.58 | 9.88 | 5.96 | 10.73 | **9.36** | 9.68 | 10.33 | 10.50 | 10.04 | 7.81 |
| h2 | 12.59 | 9.88 | 18.03 | 10.99 | **9.36** | 9.68 | 10.33 | 10.51 | 10.04 | 11.71 |
| objF | -63.61 | -65.80 | -58.47 | -64.17 | **-66.50** | -65.20 | -65.26 | -63.94 | -65.79 | -63.42 |
| | | | | | | | | | | |
| Results | x1 | x2 | x3 | x4 | x5 | x6 | x7 | x8 | x9 | x10 |
| tau | 0.09 | 0.09 | 0.09 | 0.09 | **0.09** | 0.09 | 0.09 | 0.09 | 0.09 | 0.09 |
| mc | 0.51 | 0.40 | 0.65 | 0.46 | **0.36** | 0.43 | 0.41 | 0.49 | 0.40 | 0.45 |
| ms | 0.14 | 0.11 | 0.31 | 0.15 | **0.11** | 0.12 | 0.13 | 0.14 | 0.12 | 0.23 |
| mw | 0.03 | 0.03 | 0.03 | 0.03 | **0.03** | 0.03 | 0.03 | 0.03 | 0.03 | 0.03 |
| Lw | 66.36 | 69.49 | 61.92 | 67.76 | **71.68** | 68.17 | 69.03 | 67.34 | 69.48 | 71.82 |
| ls | 0.53 | 0.50 | 0.57 | 0.52 | **0.49** | 0.51 | 0.51 | 0.52 | 0.50 | 0.49 |
| Ba | 1.49 | 1.50 | 1.50 | 1.50 | **1.44** | 1.50 | 1.50 | 1.50 | 1.50 | 1.29 |
| Bb | 1.18 | 1.27 | 1.42 | 1.24 | **1.24** | 1.27 | 1.25 | 1.25 | 1.26 | 1.18 |
| Bc | 0.82 | 0.97 | 1.36 | 0.97 | **0.99** | 0.99 | 0.97 | 0.94 | 0.97 | 1.07 |
| Bd | 0.71 | 0.88 | 0.95 | 0.87 | **0.91** | 0.89 | 0.88 | 0.83 | 0.87 | 0.96 |
| Be | 0.71 | 0.88 | 0.61 | 0.83 | **0.91** | 0.89 | 0.86 | 0.83 | 0.86 | 0.78 |
| Bf | 0.62 | 0.76 | 0.47 | 0.70 | **0.78** | 0.78 | 0.73 | 0.73 | 0.75 | 0.62 |
| Bg | 0.52 | 0.63 | 0.39 | 0.59 | **0.65** | 0.66 | 0.61 | 0.62 | 0.62 | 0.52 |
| Bh | 1.50 | 1.50 | 1.50 | 1.50 | **1.50** | 1.50 | 1.50 | 1.50 | 1.50 | 1.50 |
| Fd | 80.00 | 80.00 | 80.00 | 80.00 | **80.00** | 80.00 | 80.00 | 80.00 | 80.00 | 80.00 |
| Nc | 805.64 | 853.95 | 697.51 | 837.86 | **857.45** | 854.01 | 846.63 | 850.73 | 850.61 | 850.61 |
| objF | -63.61 | -65.80 | -58.47 | -64.17 | **-66.50** | -65.20 | -65.26 | -63.94 | -65.79 | -65.79 |
| Rc | 22.71 | 23.78 | 21.19 | 23.19 | **24.53** | 23.33 | 23.62 | 23.05 | 23.78 | 24.58 |
| Ws | 6.34 | 6.06 | 6.79 | 6.21 | **5.87** | 6.17 | 6.10 | 6.25 | 6.06 | 5.86 |
| M | 0.67 | 0.54 | 0.98 | 0.64 | **0.51** | 0.58 | 0.58 | 0.65 | 0.54 | 0.71 |
| Ls | 47.89 | 39.95 | 53.20 | 45.10 | **36.78** | 43.13 | 41.15 | 49.00 | 39.77 | 42.74 |
| Lc | 143.68 | 119.84 | 159.60 | 135.29 | **110.34** | 129.39 | 123.46 | 147.01 | 119.30 | 128.23 |